



# Phase equilibria and diffusion coefficients in the Fe-Zn binary system

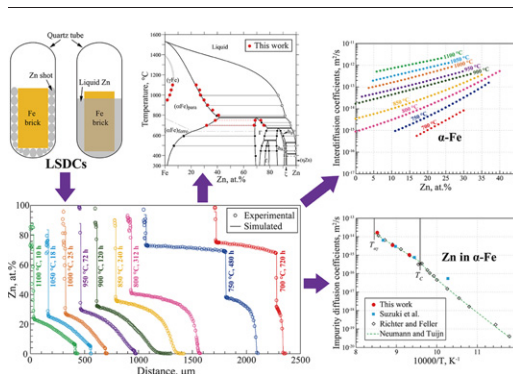
Lilong Zhu, Shreyas Honrao, Biswas Rijal, Richard G. Hennig, Michele V. Manuel \*

Department of Materials Science and Engineering, University of Florida, Gainesville, FL 32611, USA

## HIGHLIGHTS

- Phase equilibria and diffusion coefficients in the Fe-Zn system were investigated using Fe/Zn liquid-solid diffusion couples.
- Seventeen reliable equilibrium compositions of the  $\alpha$ -Fe and  $\Gamma$  phases between 700 and 1100 °C were determined.
- Interdiffusion coefficients in  $\alpha$  and  $\Gamma$  were extracted over the entire solubility range using forward-simulation analysis.
- Temperature dependence of Zn impurity diffusion coefficients in both ferromagnetic and paramagnetic  $\alpha$ -Fe was established.
- DFT calculations using different exchange-correlation functionals were performed to study Zn impurity diffusion in  $\alpha$ -Fe.

## GRAPHICAL ABSTRACT



## ARTICLE INFO

### Article history:

Received 9 August 2019

Received in revised form 30 November 2019

Accepted 16 December 2019

Available online 17 December 2019

### Keywords:

Fe-Zn system

Coating

Fe/Zn LSDCs

Phase equilibria

Diffusion coefficients

DFT calculations

## ABSTRACT

Phase diagram and diffusion coefficients of the Fe-Zn binary system are required to predict and control the microstructure of galvanized zinc coatings and thus were systematically investigated in the temperature range from 700 to 1100 °C using nine novel Fe/Zn liquid-solid diffusion couples (LSDCs). The equilibrium compositions of the  $\alpha$  and  $\Gamma$  phases of the Fe-Zn system were determined and agree well with the recently established Fe-Zn phase diagram. The extracted interdiffusion coefficients in  $\alpha$ -Fe at temperatures between 700 and 1100 °C and in  $\Gamma$  at 750 and 700 °C using the forward-simulation analysis (FSA) extend the experimental interdiffusivity measurements to the whole solubility range of these two phases. Three impurity diffusion coefficients of Zn in paramagnetic  $\alpha$ -Fe were also determined by the FSA and show good agreement with the literature data. The temperature dependence of the Zn impurity diffusion coefficients in both the paramagnetic and ferromagnetic  $\alpha$ -Fe phases across the Curie temperature  $T_C$  was established by analyzing the reliable experimental results as well as by density functional theory (DFT) calculations. The newly measured phase equilibrium and diffusivity data provide reliable inputs for future thermodynamic and kinetic modeling of the Fe-Zn system.

© 2019 Published by Elsevier Ltd. This is an open access article under the CC BY-NC-ND license (<http://creativecommons.org/licenses/by-nc-nd/4.0/>).

## 1. Introduction

Iron and steel dominate the market of metallic structural materials due to their competitive advantages including relatively low cost, high

\* Corresponding author.

E-mail address: [mmanuel@mse.ufl.edu](mailto:mmanuel@mse.ufl.edu) (M.V. Manuel).

strength-to-weight ratio and superior prefabrication [1,2]. A main drawback is the susceptibility to corrosion in most environments when left unprotected. Consequently, efforts are being made worldwide and numerous technologies have been developed to protect iron and steel from electrochemical corrosion. Among them, hot-dip galvanized coatings fabricated by immersing iron or steel in a bath of molten zinc appear as an effective and economical method that is predominantly applied for protection against corrosion [3–5]. During a hot-dip galvanizing process, iron reacts with liquid zinc to form a tightly bonded alloy coating, which consists of a series of Fe-Zn intermetallic phases, such as  $\zeta$ -FeZn<sub>13</sub>,  $\delta$ -FeZn<sub>7–10</sub>,  $\Gamma_1$ -Fe<sub>11</sub>Zn<sub>40</sub> and  $\Gamma$ -Fe<sub>3</sub>Zn<sub>10</sub> [6–8]. Phase equilibrium relations as well as diffusivity data of the Fe-Zn system are of fundamental importance to predict and control the microstructure of galvanized coatings, and thus have been extensively studied over the past century.

Experimental studies towards constructing the Fe-Zn binary phase diagram have been carried out by a number of authors and the literature data up to 1993 was carefully reviewed by Burton and Perrot [9]. Since then, the system has been thermodynamically assessed by several groups [10–15] using the CALPHAD (CALCulation of PHase Diagrams) method. More recently, Han et al. [16] re-determined the phase equilibria in the Fe-Zn phase diagram using alloy samples prepared by multi-step melting and heat treatment procedures. A new Fe-Zn phase diagram was established based on the results from electron probe micro-analyzer (EPMA), energy dispersive spectroscopy (EDS), Vickers hardness and thermal analysis, which shows a significant increase in the solubility range of the liquid and intermetallic phases compared to the previous phase diagrams.

The interdiffusion coefficients in bcc Fe-Zn ( $\alpha$ -Fe) alloys were successively investigated by Azuma et al. [17,18], Suzuki et al. [19], Budurov et al. [20,21] and Richter and Feller-Kniepmeier [22]. In all the studies, vapor-solid diffusion couples (VSDCs) were fabricated by taking advantage of the very high vapor pressure of Zn at elevated temperatures. Concentration profiles were collected by performing EPMA measurements across the entire diffusion region and the Boltzmann-Matano method was utilized to analyze the diffusivity. A brief summary of the interdiffusion coefficient data obtained by the above four groups is made in Table 1. In addition, Richter and Feller-Kniepmeier [22] obtained the impurity diffusion coefficients of Zn in bcc Fe by extrapolating the interdiffusion coefficients to pure Fe concentration. Those experimental impurity diffusion coefficients were then well assessed and documented in Neumann and Tuijn's handbook [23]. Based on the experimental results reported in the literature, Wang et al. [24] recently established the atomic mobilities in the bcc phase of the Fe-Zn system in the CALPHAD framework.

As detailed above, the Fe-Zn phase diagram as well as the diffusion coefficients in the bcc phase of the Fe-Zn system were frequently studied in the literature. The newly proposed Fe-Zn phase diagram [16] clearly defined the phase boundaries of the liquid and intermetallic phases, and thus, provides an opportunity for more accurate thermodynamic modeling of this binary system. The impurity and interdiffusion coefficients in the bcc phase of the Fe-Zn system were measured by VSDC experiments and Boltzmann-Matano analysis. However, as can be read from Table 1, the literature reported interdiffusion coefficients in the bcc phase of the Fe-Zn system are limited in a very narrow composition range. The atomic mobility database established by Wang et al.

[24] based on those limited experimental diffusivity data may not provide an accurate prediction of the diffusion behavior of Zn in Fe. Therefore, more experimental interdiffusion coefficient data are still needed to improve the atomic mobilities of the Fe-Zn system.

The diffusion couple/multiple approach [25], which enables effective collection of concentration profiles by performing EPMA analysis across the diffusion zone, is commonly utilized to efficiently determine phase diagrams on the basis of the local equilibrium assumption at the phase boundaries [26] and to rapidly measure concentration-dependent interdiffusion coefficients. Diffusion studies are usually carried out via solid-solid diffusion couples (SSDCs) that are fabricated by bringing two or more metals (pure elements or alloys) in intimate interface contact. In order to design and fabricate a successful SSDC, efforts need to be taken to avoid liquid formation in any part of an SSDC. This is especially true when studying a system with low eutectic temperatures or containing elements with low melting points. Recently, Zhong and Zhao [27,28] developed a novel method by integrating liquid-solid diffusion couple (LSDC) experiments with forward-simulation analysis (FSA) [29–32]. So far, this combined LSDC and FSA approach has been successfully applied to extract diffusion coefficients of the Mg-X (X = Al, Ca, Ce, Gd, Mn, Sn, Y, Zn) [27,28,33] and Ti-Sn [34] binary systems, showing great availability in determining high-temperature diffusion coefficients in alloy systems with low eutectic points or low melting point alloying elements.

The present study intends to collect more data on the phase equilibria and diffusion coefficients for the Fe-Zn binary system. Zn has very low melting and boiling points ( $T_m = 419\text{ }^\circ\text{C}$  and  $T_b = 907\text{ }^\circ\text{C}$ ) compared to those of Fe ( $T_m = 1538\text{ }^\circ\text{C}$  and  $T_b = 2862\text{ }^\circ\text{C}$ ). Due to the very high vapor pressure of Zn at elevated temperatures, it is challenging to cast Fe-Zn alloys by frequently-used arc melting or induction melting. As a consequence, a lot of effort had been made by previous authors to prepare the Fe-Zn samples for phase equilibrium and diffusivity studies. In the work by Han et al. [16], very skillfully but complicated procedures involving melting, re-melting, intermediate heat treatment and final heat treatment were applied to prepare Fe-Zn alloys for determining the Fe-Zn phase diagram. Since it is not feasible to prepare Fe/Zn or Fe/Fe-Zn alloy SSDCs for high-temperature heat treatments, all the previous diffusion studies were carried out by fabricating Fe/Zn VSDCs [17–22]. However, the VSDC approach failed to determine the diffusion coefficients at higher Zn concentrations. Previous work [27,28,33,34] developed a combined LSDC and FSA approach to evaluate diffusion coefficients at elevated temperatures in alloy systems with low-eutectic points or containing alloying elements with very low melting point. The present work is to apply this combined approach to the systems containing alloying elements with low melting point and high vapor pressure, such as Zn. A new but much simpler geometry was designed and used in this study to successfully fabricate the Fe-Zn LSDCs. Nine Fe/Zn LSDCs were prepared and heat treated at temperatures from 700 to 1100 °C. Concentration profiles were collected using EPMA and then used to extract phase equilibrium compositions (tie-lines) and diffusion coefficients. DFT calculations using the Vienna Ab-initio Software Package (VASP) [35–38] were also performed to provide a mechanistic understanding of the impurity diffusivities of Zn in  $\alpha$ -Fe. The data obtained in this study will help to validate and improve the Fe-Zn phase diagram and extend the diffusion coefficients of the Fe-Zn system to a much wider composition range.

**Table 1**

Summary of the literature reported chemical/interdiffusion coefficient data in the bcc phase of the Fe-Zn binary system [17–22].

Diffusion couple	Temperature range (°C)	Composition range for interdiffusion coefficients (at.% Zn)	References
Zn/Fe	915–1000	1–12	Azuma et al. [17,18]
Zn/Fe	700–980	1–20	Suzuki et al. [19]
Zn/Fe-11 at.% Zn	950–1151	11	Budurov et al. [20]
Zn/Fe-9 at.% Zn	1105	9	Budurov and Kovachev [21]
Zn/Fe	575–896	0–12	Richter and Feller-Kniepmeier [22]

## 2. Approaches

### 2.1. Experimental

A set of nine identical Fe/Zn LSDCs were prepared to study the phase equilibria and diffusion coefficients in the Fe-Zn binary system. The geometry of these LSDCs are schematically shown in Fig. 1 (a) and (b). The raw pure metals were Fe pieces with a purity of 99.97 wt% and Zn shots with a purity of 99.99 wt%. Fe ingots were first cast by arc melting the Fe pieces under an argon atmosphere using a non-consumable tungsten electrode in a water-cooled copper hearth. The Fe ingots were ground, encapsulated in evacuated quartz tubes backfilled with high-purity argon and then heat treated at 1000 °C for 120 h or 890 °C for 500 h to promote grain growth. After annealing, the Fe ingots were cut to bricks with dimensions of approximately 8 mm × 8 mm × 16 mm. The cutting surfaces were mechanically ground to 1200-grit SiC sand

paper to get a flat surface finish. Then the Fe bricks and Zn shots were ultrasonically cleaned in isopropanol and dried with compressed air.

Finally, the Fe/Zn LSDCs were assembled according to the schematic diagram shown in Fig. 1 (a). Zn shots were first put into a quartz tube (with an inner diameter of ~17 mm) until the cambered bottom was completely covered. Then an Fe brick was carefully placed onto those Zn shots, while the side gaps between the Fe brick and quartz tube were subsequently filled by adding more Zn shots. Once completing the assembly, the quartz tube containing the Fe brick and Zn shots was sealed with 1/5 atmospheric pressure argon to prevent the Fe brick and the melted Zn from being oxidized during the annealing at elevated temperatures. Following the above steps, nine Fe/Zn diffusion couple assemblies were fabricated and annealed individually at nine temperatures ranging from 700 to 1100 °C in steps of 50 °C. The heat treatment temperatures and the corresponding durations are listed in Table 2. When being annealed at a temperature above the melting point of Zn (419 °C), the Zn shots melt quickly and form a liquid pool surrounding the Fe brick as schematically shown in Fig. 1 (b). Extensive interdiffusion takes place between the Fe brick and the surrounding Zn liquid, promoting the formation of Fe solid solution ( $\alpha$ ,  $\gamma$  or both) and intermetallic phases adjacent to the liquid/solid interface. The liquid Zn solidifies when the LSDC is quenched to room temperature.

After the diffusion heat treatments listed in Table 2, the quartz tubes with the Fe/Zn LSDCs inside were quenched in water by quickly breaking the tubes. The LSDCs were then cut into equal halves through the center line of each Fe brick. One half of each LSDC was mounted in epoxy, ground and polished for further characterization by following standard metallographic sample preparation techniques. One example of a mounted Fe/Zn LSDC after annealing at 900 °C for 120 h is shown in Fig. 1 (c), where the solidified liquid Zn and Fe brick can be clearly observed. Optical microscopy (OM) and scanning electron microscopy (SEM) with local EDS were used to analyze the microstructure of the diffusion region and the phase formation by interdiffusion. Quantitative concentration profiles along the diffusion direction were measured using a CAMECA SXFiveFE EPMA with an accelerating voltage of 15 kV and a probe current of 20 nA. The step size of each EPMA measurement was carefully selected based on EDS line scan results to enable reliable equilibrium composition and diffusion coefficient analyses.

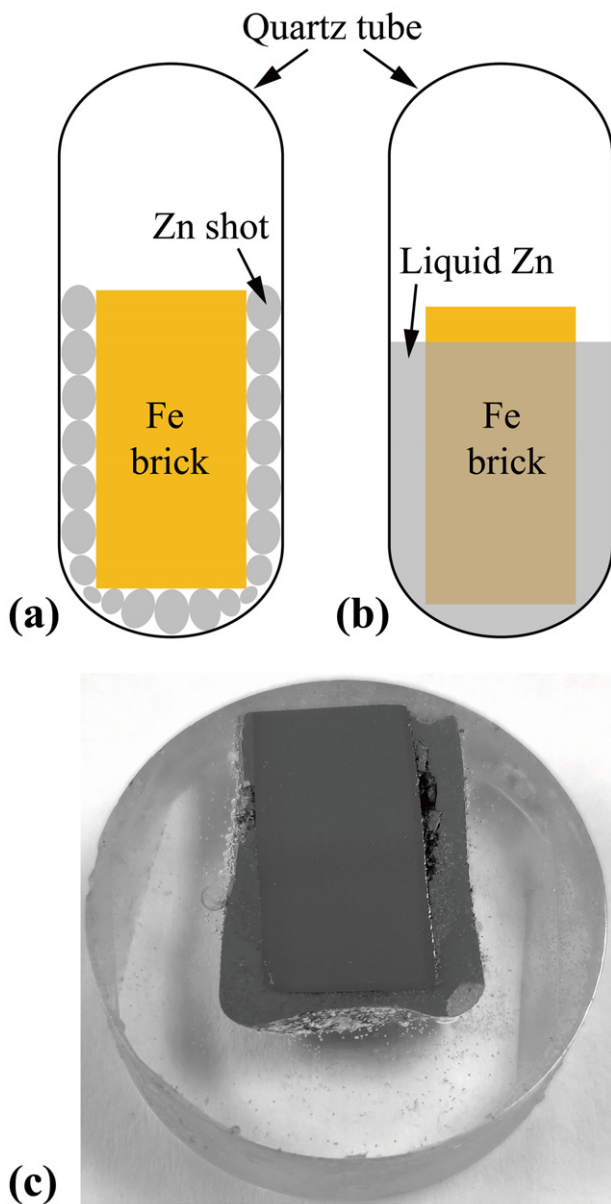


**Fig. 1.** Geometry of the Fe/Zn liquid-solid diffusion couple (LSDC): schematic diagram shows the fabrication of the LSDC (a) after encapsulation and (b) during the diffusion heat treatment; and (c) photograph of the mounted Fe/Zn LSDC after annealing at 900 °C for 120 h.

### 2.2. Computational

In recent years, first-principles calculations based on DFT have been extensively applied to calculate impurity diffusivities of a wide variety of substitutional solutes in dilute  $\alpha$ -Fe alloys [39–47]. We employed similar DFT calculations in this work to study the diffusion of Zn in ferromagnetic  $\alpha$ -Fe. These calculations were performed using the VASP with the projector augmented-wave (PAW) method [48,49]. For the exchange-correlation (XC) functional, we employed the Perdew-Burke-Ernzerhof (PBE) generalized gradient approximation (GGA) [50] and the meta-GGA approximation SCAN [51]. The SCAN functional includes information about the second derivative of the charge density and we validate its applicability to solute diffusion in  $\alpha$ -Fe. The Brillouin zone integration was conducted using the Monkhorst-Pack scheme with a  $4 \times 4 \times 4$   $k$ -point mesh [52]. The kinetic energy cutoff for the plane-wave basis was set to 400 eV for the structural relaxations and the nudged elastic band (NEB) calculations [53] of the migration barriers. The atoms were relaxed until the Hellman-Feynmann forces were less than 0.1 eV/Å and the energy differences were below 0.1 meV. A  $5 \times 5 \times 5$  supercell of Fe was used to reduce any possible finite-size effects. All the calculations were spin-polarized to account for the ferromagnetic nature of  $\alpha$ -Fe.

To study the Zn diffusion in  $\alpha$ -Fe, we first created an Fe vacancy in the supercell. Then, one of the neighboring Fe atoms was replaced with Zn to create a supercell with a Zn-V defect. The DFT energy of the created supercell was calculated and the reference chemical potentials for Fe and Zn were obtained from the DFT energies of pure Fe and Zn

**Table 2**  
Annealing temperatures and corresponding durations of grain growth and diffusion heat treatment conditions, as well as the extracted phase equilibrium compositions from the Fe-Zn LSDCs.

Grain growth heat treatment conditions for pure Fe		Diffusion heat treatment conditions for Fe/Zn LSDCs		Equilibrium phases		Equilibrium compositions (at.% Zn)	
Temp. (°C)	Time (h)	Temp. (°C)	Time (h)	Phase 1	Phase 2	Phase 1	Phase 2
1000	120	1100	10	Liquid	$\alpha$ -Fe	–	23.8
				$\alpha$ -Fe	$\gamma$ -Fe	5.9	–
1000	120	1050	18	Liquid	$\alpha$ -Fe	–	26.5
				$\alpha$ -Fe	$\gamma$ -Fe	4.8	–
1000	120	1000	25	Liquid	$\alpha$ -Fe	–	27.0
				$\alpha$ -Fe	$\gamma$ -Fe	3.7	–
1000	120	950	72	Liquid	$\alpha$ -Fe	–	29.8
				$\alpha$ -Fe	$\gamma$ -Fe	1.8	–
890	500	900	120	Liquid	$\alpha$ -Fe	–	32.6
890	500	850	240	Liquid	$\alpha$ -Fe	–	36.4
890	500	800	312	Liquid	$\alpha$ -Fe	–	40.9
890	500	750	480	Liquid	$\Gamma$	–	73.1
				$\Gamma$	$\alpha$ -Fe	68.8	38.3
890	500	700	720	Liquid	$\Gamma$	–	75.4
				$\Gamma$	$\alpha$ -Fe	67.9	31.7

to determine the formation energy ( $E^f$ ) of the Zn-V defect. Next, the NEB method in VASP was employed to calculate the migration barrier ( $E^{mig}$ ) for the Zn atom to hop into the neighboring Fe vacancy. The total activation energy of impurity diffusion ( $Q^f$ ) is then expressed as the sum of the formation energy of the Fe-Zn defect ( $E^f$ ) and the migration energy for solute-vacancy exchange ( $E^{mig}$ ), i.e.,  $Q^f = E^f + E^{mig}$ .

### 3. Results and discussion

#### 3.1. Phase equilibria of $\alpha$ -Fe and $\Gamma$

The Fe-Zn binary phase diagram [9,16] shows that the  $\gamma$ -Fe phase is stable in the temperature range from 912 to 1394 °C and the  $\Gamma$  phase is stable at temperatures below ~780 °C. Therefore, three different types of microstructures could be expected to form in the Fe/Zn LSDCs after the heat treatments at temperatures from 700 to 1100 °C: three phase layers of solidified liquid,  $\alpha$ -Fe, and  $\gamma$ -Fe in the samples annealed at 1100, 1050, 1000 and 950 °C; two phase layers of solidified liquid and  $\alpha$ -Fe in the samples annealed at 900, 850 and 800 °C; while three phase layers of solidified liquid,  $\Gamma$ , and  $\alpha$ -Fe in the samples annealed at 750 and 700 °C. Fig. 2 shows typical SEM BSE images taken from the diffusion region of three representative Fe/Zn LSDCs that were annealed at 1100, 900 and 750 °C for 10, 120 and 480 h, respectively. EPMA line scans across the entire diffusion region were performed perpendicular to the phase interfaces. All the collected concentration profiles are presented as open circles in Fig. 3.

Based on the assumption that local phase equilibria [26] are established at the phase interfaces in the diffusion region, equilibrium tie-lines can be reliably extracted by extrapolating the concentration profiles to the phase interfaces using simple straight lines. When the Fe/Zn LSDCs were quenched to room temperature, liquid Zn solidified into an inhomogeneous two-phase microstructure, Fig. 2. The phase segregation in solidified liquid results in a large variation in the measured compositions using EPMA point analysis, as shown in the upper portion of Fig. 3. It is therefore impossible to determine the exact equilibrium composition of Zn liquid phase at equilibrated annealing temperatures. Besides, in the temperature range between 950 and 1100 °C, the concentration profiles measured for Zn concentrations between the solubility limits in  $\gamma$ -Fe and pure Fe are exceedingly sharp, as can be clearly seen in Fig. 3(b). Due to the limited spatial resolution of EPMA, usually 1  $\mu$ m, composition data points obtained from these steep concentration gradient zones are insufficient, making it difficult to extrapolate to the local equilibrium compositions of  $\gamma$ -Fe accurately. Therefore, the equilibrium composition of the Zn-rich liquid phase and the solubility limit of  $\gamma$ -Fe remain unknown.

The concentration profiles obtained from the  $\alpha$ -Fe and  $\Gamma$  phase layers were extrapolated to obtain reliable equilibrium compositions. Table 2 summarizes the seventeen extracted equilibrium compositions of the  $\alpha$ -Fe and  $\Gamma$  phases. Fig. 4 compares these equilibrium compositions with the Fe-Zn binary phase diagram proposed by Han et al. [16]. The excellent agreement demonstrates the reliability and high efficiency of LSDCs for evaluating phase equilibria at elevated temperatures. In addition, the current results confirm the lowest solubility limits of  $\alpha$ -Fe, beside the  $\gamma$  loop on the left side of the phase diagram, that were assessed by Burton and Perrot [9].

#### 3.2. Interdiffusion coefficients in $\alpha$ -Fe and $\Gamma$

Based on the EPMA concentration profiles collected from the nine Fe/Zn LSDCs shown in Fig. 3, the interdiffusion and impurity diffusion coefficients were extracted using the FSA method. As mentioned above, the inhomogeneous solidified microstructure of the liquid Zn results in a large variation in the measured compositions. Such scattered liquid compositions cannot be applied directly for diffusion coefficient evaluation. Since liquid phases usually have much higher diffusion coefficients (on the order of  $10^{-9}$  to  $10^{-8}$  m<sup>2</sup>/s) than those of solid phases, the liquid Zn should have been a homogenous single-phase liquid during the entire diffusion heat treatment. Moreover, the liquid composition was assumed to be the equilibrium liquidus composition that could be defined accordingly from the Fe-Zn binary phase diagram at each annealing temperature. Considering any possible uncertainty in the proposed equilibrium liquidus composition, FSA was performed by intentionally shifting the liquid composition from 10 at.% above and below the liquidus composition. It is found that the assumed liquid composition has a negligible effect on the extracted diffusion coefficients in the solid phases. As can be seen in Fig. 3(c), the concentration profiles become extremely steep when the Zn concentrations are below 11 at.% at 750 °C and 17 at.% at 700 °C. According to the Fe-Zn phase diagram [9,16], a magnetic transition happens in  $\alpha$ -Fe at temperatures below 770 °C. The transition compositions on the magnetic transition line at 750 and 700 °C were acquired as ~3.3 and 11.5 at.% Zn, respectively, from the Fe-Zn phase diagram. Therefore, it is speculated that the steep concentration gradients at the two temperatures may be due to the magnetic transition between the paramagnetic and ferromagnetic  $\alpha$ -Fe phases.

A recent work by Chen and Zhao [54] comprehensively studied the influence of concentration gradients in the measured diffusion concentration profiles on the evaluated diffusion coefficients. They found the extracted diffusion coefficients from very steep gradient regions can be inflated by up to three orders of magnitude and recommended to

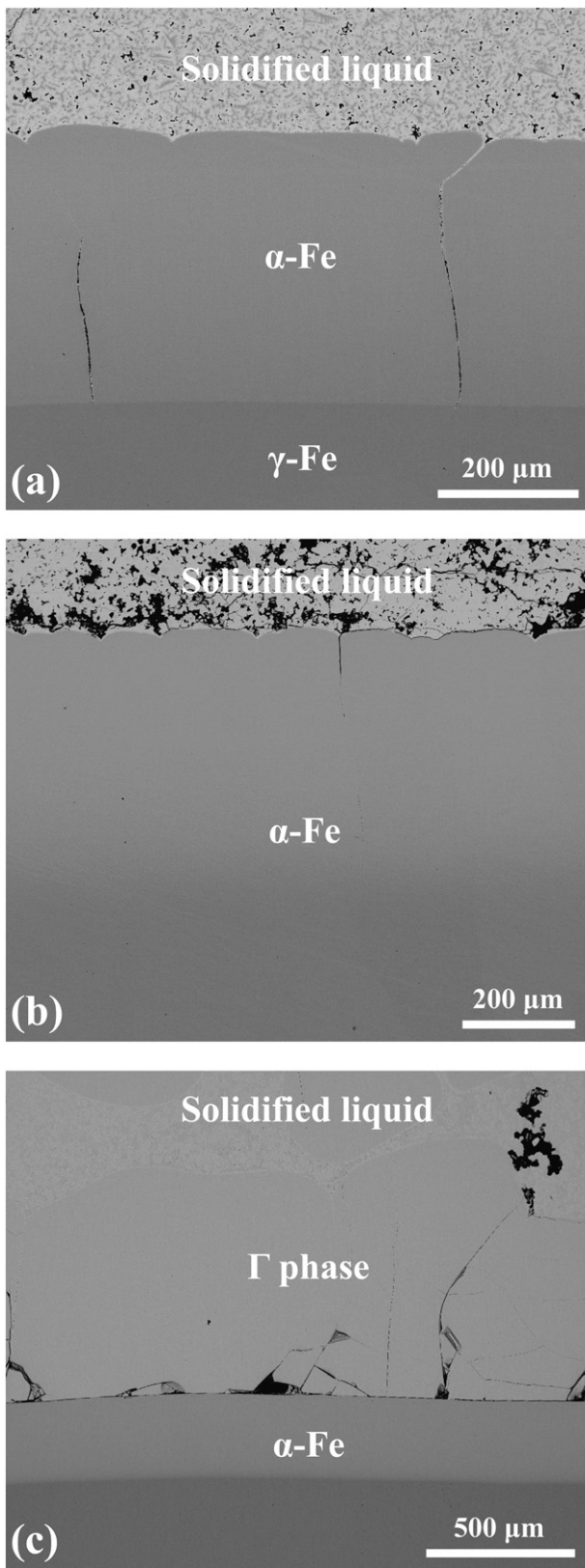


**Fig. 2.** Typical microstructures formed in three representative Fe/Zn LSDCs that were annealed at (a) 1100 °C for 10 h, (b) 900 °C for 120 h, and (c) 750 °C for 480 h.

trust the diffusion coefficients obtained from composition profiles with concentration gradients less than 1 at.% per micron. According to our concentration profiles at 750 and 700 °C, the concentration gradients are found to be much larger than 1 at.% per micron when the Zn

composition is below 11 and 17 at.%, respectively, Fig. 3(c). As a result, the extracted interdiffusion coefficients within the composition ranges of 0–11 at.% Zn at 750 °C and 0–17 at.% at 700 °C should be subject to large uncertainty, and are thus not reported in the present paper. Similarly, as detailed in Fig. 3(b), the Zn compositions change from the upper solubility limits of Zn in  $\gamma$ -Fe to about 0 at.% Zn in only 1–2  $\mu\text{m}$  in the temperature range between 950 and 1100 °C, resulting in extremely steep concentration gradients in the  $\gamma$  phase. Therefore, the diffusion coefficients in the  $\gamma$  phase cannot be accurately determined as well and are not reported in the present paper.

The concentration profiles simulated by the FSA are plotted as solid lines in Fig. 3, in comparison with the experimental concentration profiles (open circles). The good reproduction of the concentration profiles indicates that the extracted diffusion coefficients are reliable. Fig. 5 (a) and (b) show the measured interdiffusion coefficients in  $\alpha$ -Fe and  $\Gamma$ , respectively, as a function of Zn concentration. As can be seen, the interdiffusion coefficients in both phases increase with Zn content. It is worth mentioning that the currently obtained interdiffusion coefficients cover the entire compositions of the  $\alpha$ -Fe and  $\Gamma$  single-phase regions, while the existing literature data is only available in quite limited composition ranges, as detailed in Table 1. Fig. 6 compares the present interdiffusion coefficients in  $\alpha$ -Fe with the results reported by Suzuki et al. [19] and Richter and Feller-Kniepmeier [22] at or close to the same temperatures. The experimental results from Azuma et al. [17,18] at 1000, 950, and 915 °C show much lower values than those from Suzuki et al. and Richter and Feller-Kniepmeier, and thus are not adopted for comparison. It can be seen in Fig. 6 that our results agree well with those reported by Richter and Feller-Kniepmeier. With the considerable temperature difference, the overall agreement with the data reported by Suzuki et al. is also reasonable, except for the ones at 700 °C, which are significantly higher than our data and the data of Richter and Feller-Kniepmeier.

### 3.3. Impurity diffusion coefficients of Zn in $\alpha$ -Fe

The impurity diffusion coefficients can also be obtained using the FSA on the basis of the Darken equations [55], which show that the interdiffusion coefficients are identical to the impurity diffusion coefficients as the composition approaches pure elements. The measured impurity diffusion coefficients of Zn in paramagnetic  $\alpha$ -Fe are presented in Fig. 7, in comparison with the experimental data (open symbols) from Richter and Feller-Kniepmeier [22] as well as the data (dashed lines) assessed by Neumann and Tuijn [23]. The excellent agreement also gives very high confidence in the measured interdiffusion coefficients shown in Fig. 5. The impurity diffusion coefficients estimated by extrapolating the interdiffusion coefficients of Suzuki et al. [19] to pure Fe are also included as solid squares in Fig. 7. As can be seen, the estimated impurity diffusion coefficient at 700 °C has a much higher value compared to the data of Richter and Feller-Kniepmeier, and Neumann and Tuijn, which again suggests their interdiffusion coefficients at 700 °C are probably less reliable.

Fig. 8 provides a direct validation for the reliability of the FSA in determining diffusion coefficients from the collected concentration profiles. The vertical axis is the three extracted impurity diffusion coefficients at 900, 850, and 800 °C from the present work, while the horizontal axis is the data interpolated using the activation energy and the pre-exponential factor values that were calculated by performing the Arrhenius analysis on the experimental data from Suzuki et al. [19] and Richer and Feller-Kniepmeier [22], individually. As marked by the two black dashed lines in Fig. 8, the uncertainty in the measured impurity diffusion coefficients using FSA is within half an order of magnitude. Similar uncertainty of about half an order of magnitude may also exist in the measured interdiffusion coefficients in Fig. 5 using FSA [32,56].

The temperature-dependent impurity diffusion coefficients measured in the present study together with the experimental results

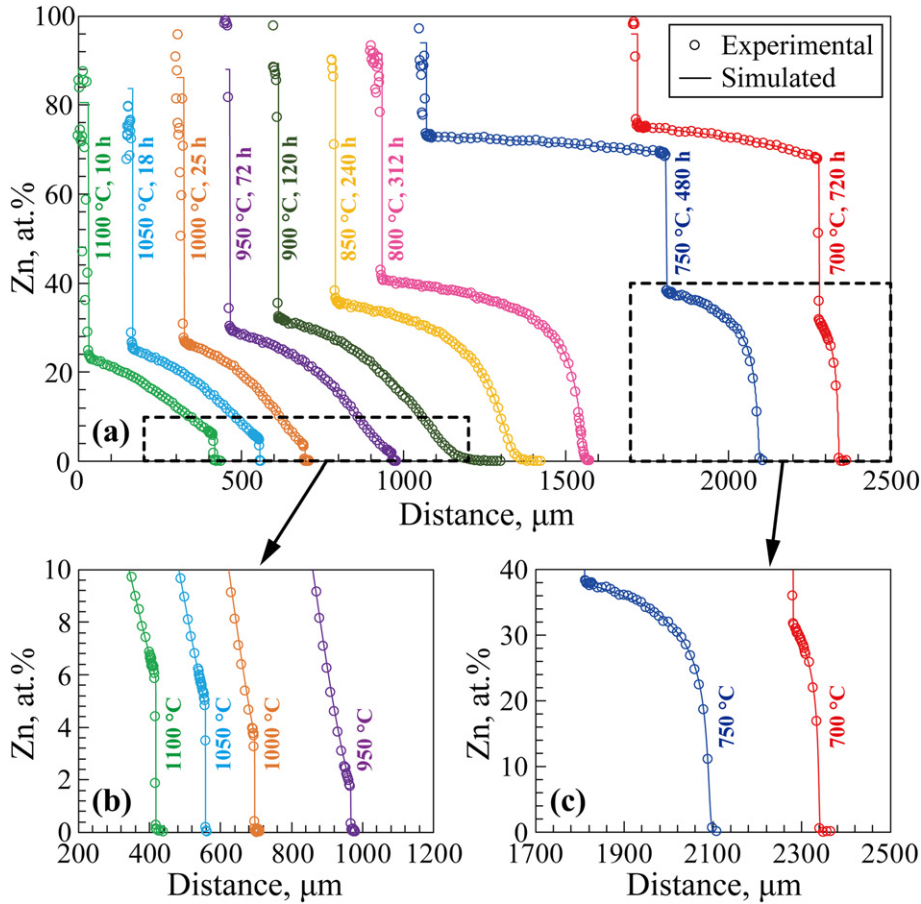


**Fig. 3.** (a) Experimentally measured concentration profiles (open circles) by performing EPMA line scans across the entire diffusion region formed in the nine Fe/Zn LSDCs, together with the corresponding profiles (solid lines) simulated using the FSA. Enlarged views are taken from the black dashed box locations in (a) to show the very steep concentration gradients (b) in the  $\gamma$  phase near the  $\alpha/\gamma$  phase interface at 1100, 1050, 1000 and 950 °C, and (c) in the  $\alpha$  phase near pure Fe side at 750 and 700 °C.

from Richer and Feller-Kniepmeier [22] allow us to perform the Arrhenius analysis. As seen in Fig. 7, the impurity diffusion coefficients of Zn in the paramagnetic  $\alpha$ -Fe (in the temperature range between the  $\alpha$ - $\gamma$  transformation temperature,  $T_{\alpha\gamma} = 1184$  K, and the Curie temperature,

$T_C = 1043$  K) show a linear Arrhenius relationship:

$$D = 4.0 \times 10^{-2} \exp\left(\frac{-280.3 \text{ kJ mol}^{-1}}{RT}\right) \text{ m}^2\text{s}^{-1} \quad (1)$$

However, the Arrhenius plot of the impurity diffusion coefficients of Zn in the ferromagnetic  $\alpha$ -Fe (below  $T_C$ ) presents a downward deviation from the Arrhenius relationship extrapolated from the paramagnetic state and an upward curvature at temperatures close to  $T_C$ . Based on the basic Bragg-Williams theory of order-disorder alloys, Ruch et al. [57] developed a model to describe such temperature dependence of the diffusion coefficients in the temperature range covering both the paramagnetic and ferromagnetic  $\alpha$ -Fe phases. The resulting model given by Ruch et al. is:

$$D = D_0^p \exp\left[-Q^p(1 + \alpha s^2)/RT\right] \quad (2)$$

where  $D_0^p$  and  $Q^p$  are the pre-exponential factor and activation energy for the diffusion in the paramagnetic  $\alpha$ -Fe phase, respectively. The coefficient  $s$  is the ratio of the spontaneous magnetization at temperature  $T$  to that at  $T = 0$  K (reduced magnetization). The values of  $s$  have been experimentally measured by Potter [58], and Crangle and Goodman [59], which vary continuously between 1 at 0 K and 0 at  $T_C$  in ferromagnetic  $\alpha$ -Fe, and  $s = 0$  for all temperatures in paramagnetic  $\alpha$ -Fe. The coefficient  $\alpha$  is a solute-dependent quantity that describes the effect of the magnetic transformation on diffusion, which can be evaluated from the

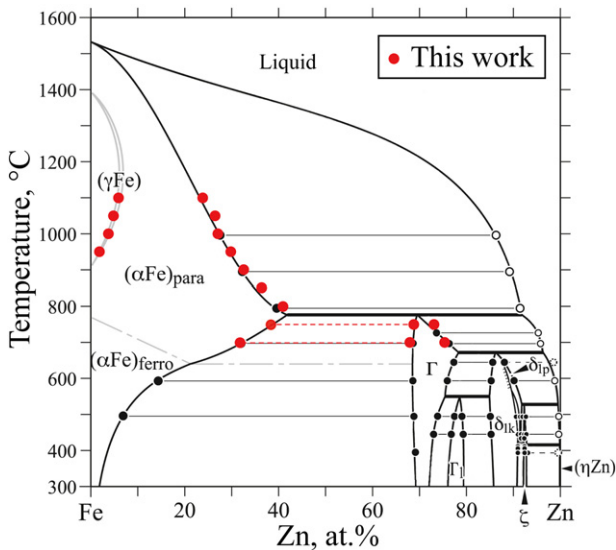


**Fig. 4.** Comparison of the equilibrium compositions of the  $\alpha$ -Fe and  $\Gamma$  phases obtained in this study with the Fe-Zn binary phase diagram proposed by Han et al. [16].

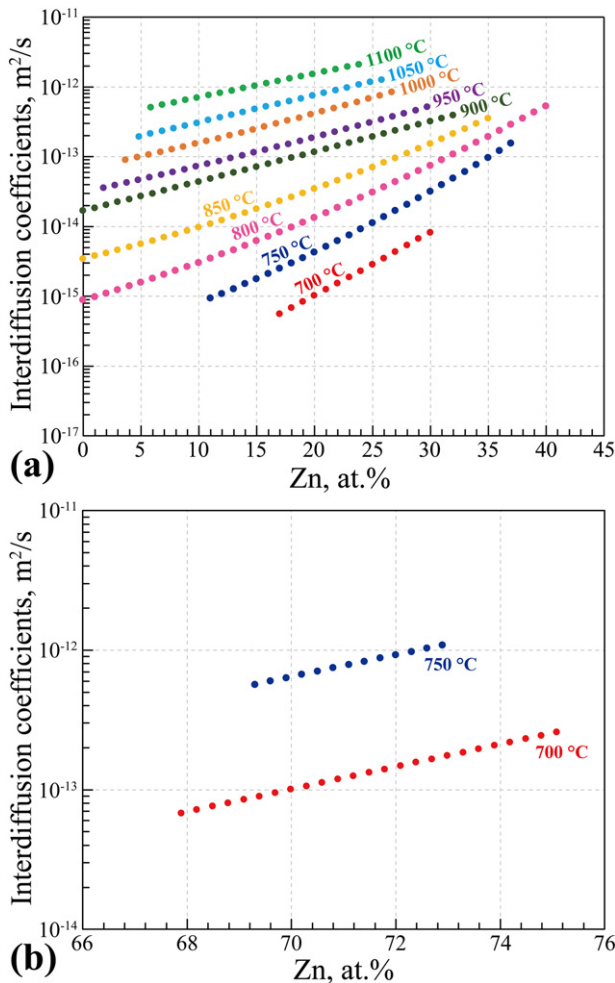


Fig. 5. Extracted interdiffusion coefficients in the Fe-Zn binary system: (a) the  $\alpha$ -Fe phase and (b) the  $\Gamma$  phase.

experimental diffusivity data by rewriting Eq. (2) as follows:

$$T \ln \frac{D}{D_0^P} = -\frac{Q^P}{R} - \frac{\alpha Q^P}{R} s^2 \quad (3)$$

Thus, a linear relationship between  $T \ln (D/D_0^P)$  and  $s^2$  can be plotted by substituting the  $D$  and  $D_0^P$  values from the experimental impurity diffusion coefficients and the  $s^2$  values from Crangle and Goodman [59],

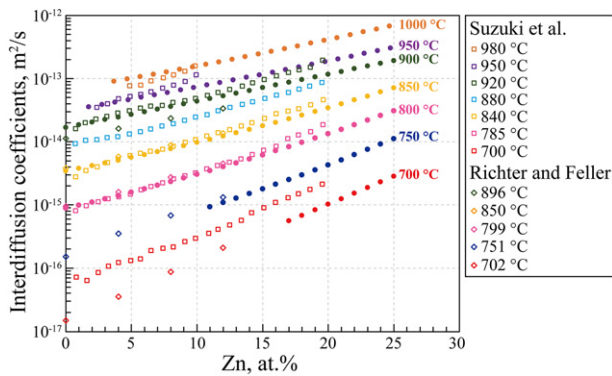


Fig. 6. Comparison of the interdiffusion coefficients in  $\alpha$ -Fe obtained from this study (solid circles) with those reported by Suzuki et al. [19] and Richer and Feller-Kniepmeier [22] (open symbols).

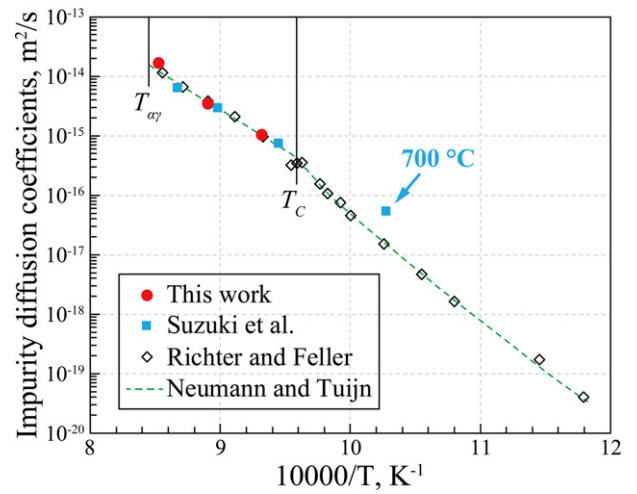


Fig. 7. Comparison of the impurity diffusion coefficients of Zn in  $\alpha$ -Fe obtained in this study with the experimental data from Suzuki et al. [19] and Richer and Feller-Kniepmeier [22] as well as the data assessed by Neumann and Tuijn [23]. The impurity diffusion coefficient data from Suzuki et al. were estimated in this work by extrapolating their interdiffusion coefficients to pure Fe.

which enables the measurement of  $\alpha$  and  $Q^P$  from the slope and intercept of the linear plot. The values of  $\alpha$  and  $Q^P$  were calculated to be 0.084 and 278.7 kJ/mol, respectively. It is noted that the  $Q^P$  obtained in this way is in good agreement with the value evaluated directly from Eq. (1), i.e., 280.3 kJ/mol.

Substituting the values of  $D_0^P = 4.0 \times 10^{-2} \text{ m}^2/\text{s}$ ,  $Q^P = 280.3 \text{ kJ/mol}$  and  $\alpha = 0.084$  into Eq. (2), the temperature dependence of the impurity diffusion coefficient of Zn in  $\alpha$ -Fe can be expressed by

$$D = 4.0 \times 10^{-2} \exp \left[ -\frac{280.3 \text{ kJ mol}^{-1} \cdot (1 + 0.084s^2)}{RT} \right] \text{ m}^2/\text{s} \quad (4)$$

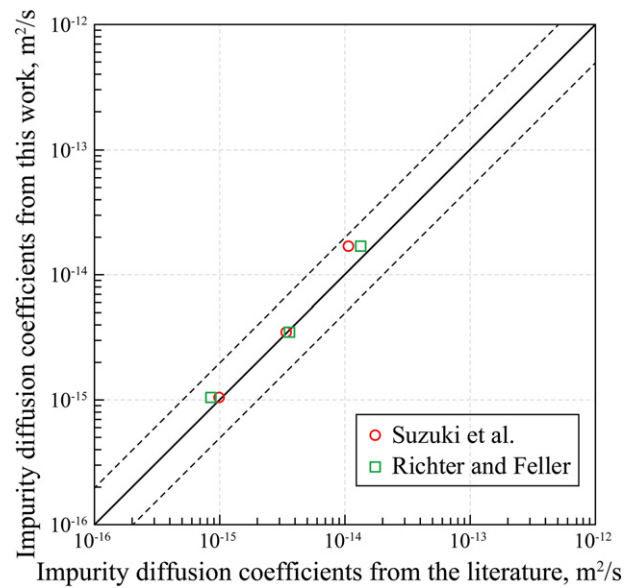


Fig. 8. The three impurity diffusion coefficients obtained from this work in comparison with those from the literature [19,22]. The literature data are interpolated using the activation energy and the pre-exponential factor calculated according to the Arrhenius equation since the exact temperature data are not available. The two black dashed lines correspond to values that are either twice or half the equal values (black solid diagonal line).

The Arrhenius plot from Eq. (4) is presented as a red solid line in Fig. 9, in comparison with the experimental results from the present work and those from Richer and Feller-Kniepmeier [22]. The Arrhenius plot of the self-diffusion coefficients in  $\alpha$ -Fe is also shown in Fig. 9 as a black solid line, using the values of  $D_0^p = 2.76 \times 10^{-4} \text{ m}^2/\text{s}$ ,  $Q^p = 250.6 \text{ kJ/mol}$  and  $\alpha = 0.156$  given by Iijima et al. [60]. It can be seen that the impurity diffusion coefficients of Zn in  $\alpha$ -Fe are about 4–7 times higher than the corresponding self-diffusion coefficients.

According to Eq. (2), the activation energy  $Q^f$  for the diffusion in the ferromagnetic  $\alpha$ -Fe at 0 K can be written as:

$$Q^f = Q^p (1 + \alpha) \quad (5)$$

Putting the  $Q^p$  and  $\alpha$  values into Eq. (5), the  $Q^f$  for Zn diffusion and self-diffusion in ferromagnetic  $\alpha$ -Fe was calculated to be 303.8 and 289.7 kJ/mol, respectively. Therefore, the increase of the activation energy in  $\alpha$ -Fe due to the magnetic transition, i.e.  $\alpha Q^p$ , is 23.5 kJ/mol for the solute diffusion of Zn, while it is 39.1 kJ/mol for the self-diffusion.

DFT calculations were also performed to study the impurity diffusion of Zn in  $\alpha$ -Fe. Table 3 summarizes our DFT calculated values of  $E^f$ ,  $E^{mig}$  and  $Q^f$  using the PBE GGA and SCAN meta-GGA XC functionals together with the  $Q^f$  values reported by Versteylet et al. [46] using PW91 and PBEsol GGA XC functionals. As expected, the two GGA XC functionals, PBE and PW91, result in almost the same values of 252.8 and 251.8 kJ/mol, respectively. However, these two GGA functionals significantly underestimate the experimental diffusion activation energy of 303.8 kJ/mol. In contrast, the calculated  $Q^f$  of 288.5 and 300.1 kJ/mol using the SCAN meta-GGA and PBEsol GGA XC functionals are much closer to the experimental results, indicating that the inhomogeneities in the charge density are significant for the solute diffusion and require approximations for the XC functionals that specifically account for these large changes in charge densities such as provided by the PBEsol and SCAN functionals.

The total diffusion activation energy for Zn diffusion in paramagnetic  $\alpha$ -Fe,  $Q^p$ , was calculated to be 233.2 and 266.1 kJ/mol, respectively, by substituting the obtained  $Q^f$  values (252.8 and 288.5 kJ/mol) and  $\alpha = 0.084$  into Eq. (5). The two  $Q^p$  values given by Versteylet et al. [46] are 228.9 and 272.3 kJ/mol, respectively. To compare the calculated diffusion activation energies using the different XC functionals with the experimental data, we obtained the pre-exponential factor for the solute diffusion by matching the diffusivity at  $T_c$ . Fig. 9 compares the DFT results (dashed lines) against the experimental measurements (symbols and red solid line). The results show good agreement for the diffusion activation energies obtained from the SCAN meta-GGA and PBEsol GGA XC functionals and a systematic underestimate of the activation energies from the PBE and PW91 GGA XC functionals. This illustrates the importance of using XC functionals that can account for the large charge density variations during diffusion via vacancies in metallic systems to accurately determine diffusion activation energies.

#### 4. Conclusions

The present work systematically investigated the phase equilibria and diffusion coefficients in the Fe-Zn binary system using a set of nine identical Fe/Zn LSDCs. The LSDCs were carefully prepared and

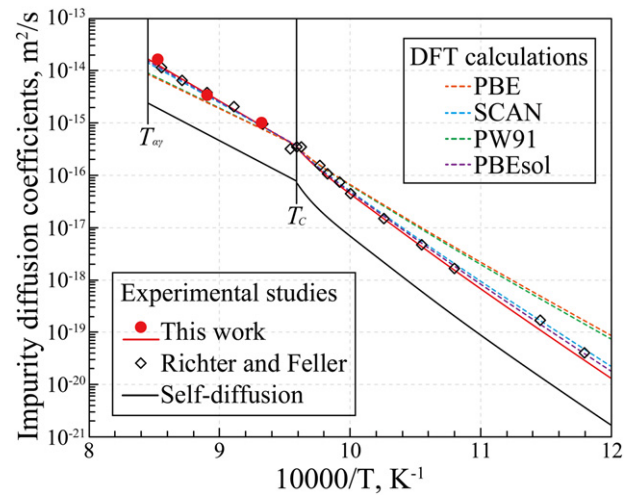


Fig. 9. Arrhenius plots of the impurity diffusion coefficients of Zn in  $\alpha$ -Fe obtained from experimental measurements and DFT calculations, in comparison with the experimental results from this work and those from Richer and Feller-Kniepmeier [22]. Arrhenius plot of the self-diffusion coefficients in  $\alpha$ -Fe reported by Iijima et al. [60] is also shown for reference. The pre-exponential factors used for these DFT plots were obtained by matching the experimental diffusivity at  $T_c$ .

heat treated at the temperatures ranging from 700 to 1100 °C. Concentration profiles were collected from the diffusion regions by performing EPMA line scans parallel to the diffusion direction, which were then utilized for phase equilibrium composition extrapolation based on the local equilibrium assumption and for diffusion coefficients extraction using FSA. A sufficiently large amount of new phase equilibrium and diffusivity data was collected for the Fe-Zn system that will help improve future thermodynamic and diffusion mobility databases of this binary system for modeling the hot-dip galvanizing process. The main conclusions drawn from the present study are summarized in the following:

- (1) Seventeen equilibrium compositions of the  $\alpha$ -Fe and  $\Gamma$  phases between 700 and 1100 °C were determined and show good agreement with the literature reported Fe-Zn phase diagram.
- (2) Composition-dependent interdiffusion coefficients in  $\alpha$ -Fe at 50 °C intervals from 700 to 1100 °C and in  $\Gamma$ -Fe<sub>3</sub>Zn<sub>10</sub> at 750 and 700 °C were extracted using FSA, expanding the experimental interdiffusivity measurements to the whole solubility range of these two phases. Three impurity diffusion coefficients of Zn in paramagnetic  $\alpha$ -Fe were also obtained using the FSA on the basis of the Darken equations.
- (3) Temperature dependence of the Zn impurity diffusion coefficients in both ferromagnetic and paramagnetic  $\alpha$ -Fe was established using the model developed by Ruch et al. The model parameters of  $D_0^p = 4.0 \times 10^{-2} \text{ m}^2/\text{s}$ ,  $Q^p = 280.3 \text{ kJ/mol}$  and  $\alpha = 0.084$  were calculated based on the impurity diffusion coefficients determined in this study and those reported in literature.
- (4) DFT calculations were also performed to study the impurity diffusion of Zn in  $\alpha$ -Fe, suggesting that the computed diffusion

Table 3

Calculated energetics for the Zn impurity diffusion in both ferromagnetic ( $Q^f$ ) and paramagnetic ( $Q^p$ )  $\alpha$ -Fe together with the computed results by Versteylet et al. [46].

Formation energy, $E^f$ (eV)	Migration energy, $E^{mig}$ (eV)	Activation energy, $Q^f$ (eV)	Activation energy, $Q^f$ (kJ/mol)	Activation energy, $Q^p$ (kJ/mol)	$\alpha$	GGA XC functional	Ref.
2.21	0.41	2.62	252.8	233.2	0.084	PBE	This work
2.56	0.43	2.99	288.5	266.1	0.084	SCAN	This work
–	–	2.61	251.8	228.9	0.1	PW91	Versteylet et al. [46]
–	–	3.11	300.1	272.3	0.1	PBEsol	Versteylet et al. [46]

activation energy is sensitive to the choice of exchange-correlation functional. The activation energies calculated using SCAN meta-GGA and PBEsol GGA XC functionals agree with the experimental measurements and confirm the vacancy diffusion mechanism for Zn in  $\alpha$ -Fe.

### CRedit authorship contribution statement

**Lilong Zhu:** Investigation, Methodology, Data curation, Writing - original draft. **Shreyas Honrao:** Software, Data curation, Writing - review & editing. **Biswas Rijal:** Software, Data curation, Writing - review & editing. **Richard G. Hennig:** Funding acquisition, Supervision, Writing - review & editing. **Michele V. Manuel:** Funding acquisition, Supervision, Writing - review & editing.

### Declaration of competing interest

The authors declare that they have no known competing financial interests or personal relationships that could have appeared to influence the work reported in this paper.

### Acknowledgment

Financial support from the U.S. the Department of Energy (DOE), Office of Energy Efficiency and Renewable Energy (EERE), under the award number DE-EE0007742 is gratefully acknowledged. The authors are thankful to Drs. Anil Sachdev and Andrew Bobel at General Motors (GM) for valuable discussions.

### Disclaimer

This paper was prepared as an account of work sponsored by an agency of the United States Government. Neither the United States Government nor any agency thereof, nor any of their employees, makes any warranty, express or implied, or assumes any legal liability or responsibility for the accuracy, completeness, or usefulness of any information, apparatus, product, or process disclosed, or represents that its use would not infringe privately owned rights. Reference herein to any specific commercial product, process, or service by trade name, trademark, manufacturer, or otherwise does not necessarily constitute or imply its endorsement, recommendation, or favoring by the United States Government or any agency thereof. The views and opinions of authors expressed herein do not necessarily state or reflect those of the United States Government or any agency thereof.

### Data availability

The raw data that supports the findings of this study is available from the corresponding author upon reasonable request.

### References

- [1] J.C. McCormac, S.F. Csemak, *Structural Steel Design*, fifth ed. Prentice Hall, New Jersey, 2012.
- [2] W.F. Hosford, *Iron and Steel*, Cambridge University Press, New York, 2012.
- [3] V. Kuklík, J. Kudláček, *Hot-dip Galvanizing of Steel Structures*, Butterworth-Heinemann, Oxford, 2016.
- [4] S.M.A. Shibli, B.N. Meena, R. Remya, A review on recent approaches in the field of hot dip zinc galvanizing process, *Surf. Coat. Technol.* 262 (2015) 210–215.
- [5] A.R. Marder, The metallurgy of zinc-coated steel, *Prog. Mater. Sci.* 45 (2000) 191–271.
- [6] J.D. Culcasi, P.R. Seré, C.I. Elsner, A.R. Di Sarli, Control of the growth of zinc-iron phases in the hot-dip galvanizing process, *Surf. Coat. Technol.* 122 (1999) 21–23.
- [7] R. Sa-nguanmoo, E. Nisaratanaporn, Y. Boonyongmaneerat, Hot-dip galvanization with pulse-electrodeposited nickel pre-coatings, *Corros. Sci.* 53 (2011) 122–126.
- [8] M.H. Razmpoosh, A. Macwan, E. Biro, D.L. Chen, Y. Peng, F. Goodwin, Y. Zhou, Liquid metal embrittlement in laser beam welding of Zn-coated 22MnB5 steel, *Mater. Design* 155 (2018) 375–383.
- [9] B.P. Burton, P. Perrot, Fe-Zn (Iron-Zinc), in: H. Okamoto (Ed.), *Phase Diagram of Binary Iron Alloys*, ASM International, Material Park, OH 1993, pp. 459–466.
- [10] G. Reumont, P. Perrot, J.M. Fiorani, J. Hertz, Thermodynamic assessment of the Fe-Zn system, *J. Phase Equilib.* 21 (2000) 371–378.
- [11] X.P. Su, N.Y. Tang, J.M. Toguri, Thermodynamic evaluation of the Fe-Zn system, *J. Alloys Compd.* 325 (2001) 129–136.
- [12] J. Nakano, D.V. Malakhov, G.R. Purdy, A crystallographically consistent optimization of the Zn-Fe system, *CALPHAD* 29 (2005) 276–288.
- [13] X.P. Su, F.C. Yin, Z. Li, N.Y. Tang, M.X. Zhao, Thermodynamic calculation of the Fe-Zn-Si system, *J. Alloys Compd.* 396 (2005) 156–163.
- [14] W. Xiong, Y. Kong, Y. Du, Z.-K. Liu, M. Selleby, W.-H. Sun, Thermodynamic investigation of the galvanizing systems, I: refinement of the thermodynamic description for the Fe-Zn system, *CALPHAD* 33 (2009) 433–440.
- [15] Y. Tang, X. Yuan, Y. Du, W. Xiong, Thermodynamic modeling of the Fe-Zn system using exponential temperature dependence for the excess Gibbs energy, *J. Min. Metall. B* 47 (2011) 1–10.
- [16] K. Han, I. Ohnuma, K. Okuda, R. Kainuma, Experimental determination of phase diagram in the Zn-Fe binary system, *J. Alloys Compd.* 737 (2018) 490–504.
- [17] K. Azuma, S. Goto, Y.C. Wu, Reactivity of zinc vapor with metals and alloys, *Nippon Kogyo Kaishi* 82 (1966) 210–213.
- [18] K. Azuma, S. Goto, Y.C. Wu, Reactivity of zinc vapor with metals and alloys (1st report) - diffusion of zinc vapor into iron and carbon steels, *Nippon Kogyo Kaishi* 83 (1967) 1011–1015.
- [19] H. Suzuki, Y. Masuda, K. Nishida, On the interdiffusion in  $\alpha$ -solid solution of the Fe-Zn system by means of a vapor method of Zn, *J. Jpn. Inst. Metals* 36 (1972) 509–513.
- [20] S. Budurov, P. Kovatchev, Z. Kamenova, Chemical diffusion of zinc into  $\gamma$ - and  $\alpha$ -iron, *Z. Metallkd.* 64 (1973) 652–654.
- [21] S. Budurov, P. Kovachev, Multiphase diffusion in iron-zinc alloys, *Doklady Bolgarskoi Akademii Nauk* 30 (1977) 1577–1580.
- [22] I. Richter, M. Feller-Kniepmeier, Diffusion of Zn in  $\alpha$ -Fe single crystals, *Phys. Status Solidi A* 68 (1981) 289–300.
- [23] G. Neumann, C. Tuijn, *Self-diffusion and Impurity Diffusion in Pure Metals: Handbook of Experimental Data*, Elsevier, Oxford, 2009.
- [24] S.Q. Wang, P. Zhou, W.B. Zhang, S.L. Cui, L.J. Zhang, M. Yin, D.D. Liu, H.H. Xu, S.H. Liu, Y. Du, Atomic mobility and diffusivity of bcc<sub>A2</sub> phase in the Fe-X (X=Cu, Si, Zn) systems, *CALPHAD* 36 (2012) 127–134.
- [25] J.-C. Zhao, *Methods for Phase Diagram Determination*, Elsevier, Oxford, 2007.
- [26] F.J.J. van Loo, Multiphase diffusion in binary and ternary solid-state systems, *Prog. Solid State Chem.* 20 (1990) 47–99.
- [27] W. Zhong, J.-C. Zhao, First experimental measurement of calcium diffusion in magnesium using novel liquid-solid diffusion couples and forward-simulation analysis, *Scripta Mater.* 127 (2017) 92–96.
- [28] W. Zhong, J.-C. Zhao, First reliable diffusion coefficients for Mg-Y and additional reliable diffusion coefficients for Mg-Sn and Mg-Zn, *Metall. Mater. Trans. A* 48 (2017) 5778–5782.
- [29] Q.F. Zhang, J.-C. Zhao, Extracting interdiffusion coefficients from binary diffusion couples using traditional methods and a forward-simulation method, *Intermetallics* 34 (2013) 132–141.
- [30] Q.F. Zhang, J.-C. Zhao, Impurity and interdiffusion coefficients of the Cr-X (X=Co, Fe, Mo, Nb, Ni, Pd, Pt, Ta) binary systems, *J. Alloy Compd.* 604 (2014) 142–150.
- [31] L.L. Zhu, Q.F. Zhang, Z.Q. Chen, C.D. Wei, G.-M. Cai, L. Jiang, Z.P. Jin, J.-C. Zhao, Measurement of interdiffusion and impurity diffusion coefficients in the bcc phase of the Ti-X (X=Cr, Hf, Mo, Nb, V, Zr) binary systems using diffusion multiples, *J. Mater. Sci.* 52 (2017) 3255–3268.
- [32] Z.Q. Chen, Z.-K. Liu, J.-C. Zhao, Experimental determination of impurity and interdiffusion coefficients in seven Ti and Zr binary systems using diffusion multiples, *Metall. Mater. Trans. A* 49 (2018) 3108–3116.
- [33] W. Zhong, J.-C. Zhao, Measurements of diffusion coefficients of Ce, Gd and Mn in Mg, *Materialia* 7 (2019), 100353.
- [34] L.L. Zhu, Z.Q. Chen, W. Zhong, C.D. Wei, G.M. Cai, L. Jiang, Z.P. Jin, J.-C. Zhao, Measurement of diffusion coefficients in the bcc phase of the Ti-Sn and Zr-Sn binary systems, *Metall. Mater. Trans. A* 50 (2019) 1409–1420.
- [35] G. Kresse, J. Hafner, Ab initio molecular dynamics for liquid metals, *Phys. Rev. B* 47 (1993) 558–561.
- [36] G. Kresse, J. Hafner, Ab initio molecular-dynamics simulation of the liquid-metal-amorphous-semiconductor transition in germanium, *Phys. Rev. B* 49 (1994) 14251–14269.
- [37] G. Kresse, J. Furthmüller, Efficient iterative schemes for ab initio total-energy calculations using a plane-wave basis set, *Phys. Rev. B* 54 (1996) 11169–11186.
- [38] G. Kresse, J. Furthmüller, Efficiency of ab-initio total energy calculations for metals and semiconductors using a plane-wave basis set, *Comput. Mater. Sci.* 6 (1996) 15–50.
- [39] S.Y. Huang, D.L. Worthington, M. Asta, V. Ozolins, G. Ghosh, P.K. Liaw, Calculation of impurity diffusivities in  $\alpha$ -Fe using first-principles methods, *Acta Mater.* 58 (2010) 1982–1993.
- [40] J.D. Tucker, R. Najafabadi, T.R. Allen, D. Morgan, Ab initio-based diffusion theory and tracer diffusion in Ni-Cr and Ni-Fe alloys, *J. Nucl. Mater.* 405 (2010) 216–234.
- [41] S. Choudhury, L. Barnard, J.D. Tucker, T.R. Allen, B.D. Wirth, M. Asta, D. Morgan, Ab-initio based modeling of diffusion in dilute bcc Fe-Ni and Fe-Cr alloys and implications for radiation induced segregation, *J. Nucl. Mater.* 411 (2011) 1–14.
- [42] D. Murali, B.K. Panigrahi, M.C. Valsakumar, C.S. Sundar, Diffusion of Y and Ti/Zr in bcc iron: a first principles study, *J. Nucl. Mater.* 419 (2011) 208–212.
- [43] H. Ding, S.Y. Huang, G. Ghosh, P.K. Liaw, M. Asta, A computational study of impurity diffusivities for 5d transition metal solutes in  $\alpha$ -Fe, *Scripta Mater.* 67 (2012) 732–735.

- [44] C. Zhang, J. Fu, R.H. Li, P.B. Zhang, J.J. Zhao, C. Dong, Solute/impurity diffusivities in bcc Fe: a first-principles study, *J. Nucl. Mater.* 455 (2014) 354–359.
- [45] X.Y. Gao, H.P. Ren, C.L. Li, H.Y. Wang, Y.P. Ji, H.J. Tan, First-principles calculations of rare earth (Y, La and Ce) diffusivities in bcc Fe, *J. Alloys Compd.* 663 (2016) 316–320.
- [46] C.D. Versteyle, N.H. van Dijk, M.H.F. Sluiter, First-principles analysis of solute diffusion in dilute bcc Fe-X alloys, *Phys. Rev. B* 96 (2017), 094105.
- [47] H.Y. Wang, X.Y. Gao, H.P. Ren, S.M. Chen, Z.F. Yao, Diffusion coefficients of rare earth elements in fcc Fe: a first-principles study, *J. Phys. Chem. Solids* 112 (2018) 153–157.
- [48] P.E. Blöchl, Projector augmented-wave method, *Phys. Rev. B* 50 (1994) 17953–17979.
- [49] G. Kresse, D. Joubert, From ultrasoft pseudopotentials to the projector augmented-wave method, *Phys. Rev. B* 59 (1999) 1758–1775.
- [50] J.P. Perdew, K. Burke, M. Ernzerhof, Generalized gradient approximation made simple, *Phys. Rev. Lett.* 77 (1996) 3865–3868.
- [51] J.W. Sun, A. Ruzsinszky, J.P. Perdew, Strongly constrained and appropriately normed semilocal density functional, *Phys. Rev. Lett.* 115 (2015), 036402.
- [52] H.J. Monkhorst, J.D. Pack, Special points for Brillouin-zone integrations, *Phys. Rev. B* 13 (1976) 5188–5192.
- [53] H. Jónsson, G. Mills, K.W. Jacobsen, Nudged elastic band method for finding minimum energy paths of transitions, in: B.J. Berne, G. Ciccotti, D.F. Coker (Eds.), *Classical and Quantum Dynamics in Condensed Phase Simulations*, World Scientific, Singapore 1998, pp. 385–404.
- [54] Z.Q. Chen, J.-C. Zhao, Recommendation for reliable evaluation of diffusion coefficients from diffusion profiles with steep concentration gradients, *Materialia* 2 (2018) 63–67.
- [55] L.S. Darken, Diffusion, mobility and their interrelation through free energy in binary metallic systems, *Trans. AIME* 175 (1948) 184–201.
- [56] Q.F. Zhang, Z.Q. Chen, W. Zhong, J.-C. Zhao, Accurate and efficient measurement of impurity (dilute) diffusion coefficients without isotope tracer experiments, *Scripta Mater.* 128 (2017) 32–35.
- [57] L. Ruch, D.R. Sain, H.L. Yeh, L.A. Girifalco, Analysis of diffusion in ferromagnets, *J. Phys. Chem. Solids* 37 (1976) 649–653.
- [58] H.H. Potter, The magneto-caloric effect and other magnetic phenomena in iron, *Proc. R. Soc. Lond. A* 146 (1934) 362–387.
- [59] J. Crangle, G.M. Goodman, The magnetization of pure iron and nickel, *Proc. R. Soc. Lond. A* 321 (1971) 477–491.
- [60] Y. Iijima, K. Kimura, K. Hirano, Self-diffusion and isotope effect in  $\alpha$ -iron, *Acta Metall.* 36 (1988) 2811–2820.